39th AIAA/ASME/SAE/ASEE Joint Propulsion Conference and Exhibit
20-23 July 2003, Huntsville, Alabama

AIAA 2003-5083

Large-Eddy Simulation of a Single-Cup Gas-Turbine Combustor Flows

V. Sankaran I. Porumbel and S. Menon
School of Aerospace Engineering
Georgia Institute of Technology
Atlanta, Georgia 30332

39th AIAA/ASME/SAE/ASEE
Joint Propulsion Conference
July 20–23, 2003 / Huntsville, Alabama

Large-Eddy Simulation of a Single-Cup Gas-Turbine Combustor Flows

V. Sankaran*I. Porumbel†and S. Menon‡
School of Aerospace Engineering
Georgia Institute of Technology
Atlanta, Georgia 30332

Abstract

A generic formulation for modeling the sub-grid combustion in compressible, high Reynolds number, two-phase, reacting flows has been developed and validated. A sub-grid mixing/combustion model called Linear Eddy Mixing (LEM) model has been extended to compressible flows and used inside the framework of Large Eddy Simulation (LES) in this LES-LEM approach. In LES-LEM, all the physical processes such as molecular diffusion, small and large scale turbulent convection and chemical reaction are modeled separately, but concurrently at their respective time scales. This multi-scale phenomena is solved using a two-scale numerical approach, wherein molecular diffusion, small scale turbulent convection and chemical reaction are grouped as small scale processes, and the convection at the (LES grid) resolved scales are deemed as the large scale processes. Small-scale processes are solved using a hybrid finite-difference Monte-Carlo type approach in a one-dimensional sub-grid domain. Large-scale advection on the three-dimensional LES grid is modeled in a Lagrangian manner that conserves mass. Validation of the compressible LES-LEM approach is conducted by simulating the flow-field in an operational General Electric Aircraft Engines combustor (LM6000). The results predicted using the proposed approach compares well with the experiments and a conventional (G-equation) thin-flame model.

1 Introduction

The modeling of turbulent fluid flow in realistic engineering geometries, even in the non-reacting case, remains a major scientific challenge. It is well known that large scale advective transport breaks down the in-homogeneity in the scalar field into smaller scales, and molecular diffusion dissipate the scalar fluctuations at small scales by acting on the local gradients. Chemical reaction and the associated heat release introduce fine-scale density and velocity fluctuations, which in turn couple the small scale events back to the larger fluid-dynamic scales. This close coupling between the various processes and the presence of wide separation between the relevant scales makes turbulent combustion modeling more complex compared to turbulent modeling for non-reacting flows.

Complete resolution of all the length and time scales involved in reactive flows is prohibitively expensive and this precludes the use of Direct Numerical simulation (DNS). On the other hand, the unreliable nature of the solution predicted by Reynolds Averaged Navier Stokes (RANS) approach in complex (unsteady, swirling) flows makes it unsuitable for combustion problems that are inherently unsteady and involve swirl and flow separation. Large-Eddy Simulation (LES) is emerging to be an alternative promising tool for studying reacting flows in complex geometries. In LES, only the flow/geometry dependent, three-dimensional large scale motion are resolved and the sub-grid, small scales that exhibit local isotropy are modeled.

So far, only a few studies have been attempted on LES of reactive flows due to the following reason. Even though the major part of the energy containing scales are resolved using LES, a sub-grid model is still needed to represent the larger unresolved scales. But it is well known that the chemical reactions and heat release occur at the smallest dissipative scales (by molecular mixing) and not at the larger resolved scales. Hence, sub-grid modeling techniques, which have successfully been used in sub-grid modeling of momentum transport are not as successful in modeling reactive scalar transport.

In this study, we report the development of a more comprehensive sub-grid combustion model for LES that attempts to simulate the various physical processes at their relevant length and time scales. Application of this model to study the reacting flow-field in an operational hardware, LM6000, Dry Low Emissions combustor is presented.

2 Governing Equations for LES

In this section, governing equations and the modeling techniques used in LES are presented. The flow variables are decomposed into the resolved (super-grid scale) and unresolved (sub-grid scale) components by a

*Graduate Research Assistant, AIAA Student Member
†Graduate Research Assistant, AIAA Student Member
‡Professor, AIAA Associate Fellow

spatial filtering operation, such that $f = \tilde{f} + f''$, where the tilde ($\sim$) denotes resolved scale and double prime ($''$) denotes unresolved sub-grid scale quantities. The Favre filtered variable is defined as $\tilde{f} = \overline{\rho f}/\bar{\rho}$ where the over-bar represents a spatial filtering, which is defined as:

$$\overline{\rho f(x_i,t)} = \int_D \rho f(z_i,t) G(x_i - z_i, \Delta) dz_i. \qquad (1)$$

Here, G is the filter kernel, D is the domain of integration and Δ is filter size, defined as $\Delta = (\Delta x \Delta y \Delta z)^{1/3}$, where Δx, Δy and Δz are the grid size in axial, transverse and spanwise directions, respectively. In this study, a box filter is employed which is appropriate for finite volume schemes.[1] The filter function G (in any direction, x) is defined as:

$$G = \begin{cases} 1/\Delta & -\frac{\Delta}{2} \le (x-z) \le \frac{\Delta}{2} \\ 0 & \text{otherwise} \end{cases} \qquad (2)$$

Applying the filtering operator to the conservation equations of mass momentum, energy and species equations results in the following LES equations for two-phase flows:

$$\begin{aligned}
&\tfrac{\partial \bar{\rho}}{\partial t} + \tfrac{\partial \bar{\rho}\tilde{u}_i}{\partial x_i} = 0 \\
&\tfrac{\partial \bar{\rho}\tilde{u}_i}{\partial t} + \tfrac{\partial}{\partial x_j}[\bar{\rho}\tilde{u}_i\tilde{u}_j + \bar{p}\delta_{ij} - \bar{\tau}_{ij} + \tau^{sgs}_{ij}] = 0 \\
&\tfrac{\partial \bar{\rho}\tilde{E}}{\partial t} + \tfrac{\partial}{\partial x_i}[(\bar{\rho}\tilde{E} + \bar{p})\tilde{u}_i + \bar{q}_i - \tilde{u}_j\bar{\tau}_{ji} + H^{sgs}_i + \sigma^{sgs}_i] = 0 \\
&\tfrac{\partial \bar{\rho}\tilde{Y}_k}{\partial t} + \tfrac{\partial}{\partial x_i}[\bar{\rho}\tilde{Y}_k\tilde{u}_i - \bar{\rho}\tilde{Y}_k\widetilde{V_{i,k}} + Y^{sgs}_{i,k} + \theta^{sgs}_{i,k}] = \bar{\dot{w}}_k
\end{aligned}$$

where $k = 1$ to N_s and N_s is the total number of species present in the system. $\bar{q}_i$ is the heat flux vector given by

$$\bar{q}_i = -\bar{\kappa}\frac{\partial \tilde{T}}{\partial x_i} + \bar{\rho}\sum_{k=1}^{N_s}\tilde{h}_k\tilde{Y}_k\widetilde{V_{i,k}} + \sum_{k=1}^{N_s} q^{sgs}_{i,k} \qquad (3)$$

The diffusion velocities are approximated using Fickian diffusion as $\widetilde{V_{i,k}} = (-\bar{D}_k/\tilde{Y}_k)(\partial\tilde{Y}_k/\partial x_i)$. The sub-grid terms that require closure are:

$$\begin{aligned}
\tau^{sgs}_{ij} &= \overline{\rho}\,(\widetilde{u_i u_j} - \widetilde{u}_i\widetilde{u}_j) \\
H^{sgs}_i &= \overline{\rho}\,(\widetilde{Eu_i} - \widetilde{E}\widetilde{u}_i) + (\overline{pu_i} - \overline{p}\widetilde{u}_i) \\
\sigma^{sgs}_i &= \widetilde{u_j\tau_{ij}} - \widetilde{u}_j\overline{\tau}_{ij}. \\
Y^{sgs}_{i,k} &= \bar{\rho}[\widetilde{u_i Y_k} - \tilde{u}_i\tilde{Y}_k] \\
q^{sgs}_{i,k} &= [\overline{h_k D_k \partial Y_k/\partial x_i} - \tilde{h}_k\tilde{D}_k\partial\tilde{Y}_k/\partial x_i] \\
\theta^{sgs}_{i,k} &= \bar{\rho}[\widetilde{V_{i,k}Y_k} - \widetilde{V}_{i,k}\widetilde{Y}_k]
\end{aligned} \qquad (4)$$

The pressure is determined from the filtered equation of state, $\bar{p} = \bar{\rho}R\tilde{T} + T^{sgs}$. Here, T^{sgs} is the temperature-species correlation term, defined as $[\widetilde{Y_k T} - \tilde{Y}_k\tilde{T}]$. For low heat-release, T^{sgs} can be expected to be negligible[2] but this may not be true for high heat release. However, due to the difficulty in modeling these terms they are generally neglected.[2,3] The filtered total energy per unit volume is given by $\bar{\rho}\tilde{E} = \bar{\rho}\tilde{e} + \frac{1}{2}\bar{\rho}\tilde{u}_i\tilde{u}_i + \bar{\rho}k^{sgs}$ where, the sub-grid kinetic energy (to be discussed later) is defined as, $k^{sgs} = (1/2)[\widetilde{u_k u_k} - \tilde{u}_k\tilde{u}_k]$. The filtered internal energy for calorically perfect gases is given by

$$\tilde{e} = \sum_{k=1}^{N_s}[c_{v,k}\tilde{Y}_k\tilde{T} + \tilde{Y}_k\Delta h^{'}_{f,k}] \qquad (5)$$

where, $\Delta h^{'}_{f,k} = \Delta h^0_{f,k} - c_{p,k}T^0$ and $\Delta h^0_{f,k}$ is the standard heat of formation at a reference temperature T^0.

2.1 Momentum Closure

Model for sub-grid stress tensor τ^{sgs}_{ij} is derived usually by drawing an analogy between the viscous stresses, (τ_{ij}) in the unfiltered Navier-Stokes equation and the sub-grid stresses, (τ^{sgs}_{ij}) in the filtered equations. Hence, the deviatoric part of the sub-grid stresses is assumed to be proportional to the deviatoric part of the resolved rate of strain, $\tilde{S}_{ij} = (1/2)(\partial\tilde{u}_i/\partial x_j + \partial\tilde{u}_j/\partial x_i)$. If the sub-grid stress tensor can be split into deviatoric and isotropic parts $\tau^{sgs}_{ij} = \tau^{sgs}_{ij,d} + \tau^{sgs}_{kk}$, then the deviatoric part $\tau^{sgs}_{ij,d}$, is modeled as follows;

$$\tau^{sgs}_{ij,d} = -2\nu_t[\tilde{S}_{ij} - \frac{1}{3}\tilde{S_{kk}}\delta_{ij}] \qquad (6)$$

Noting that $\tau^{sgs}_{kk} = (2/3)k^{sgs}\delta_{ij}$, the total sub-grid stress tensor can be expressed as

$$\tau^{sgs}_{ij} = -2\nu_t[\tilde{S}_{ij} - \frac{1}{3}\tilde{S_{kk}}\delta_{ij}] + \frac{2}{3}\bar{\rho}k^{sgs}\delta_{ij} \qquad (7)$$

Therefore, to complete the closure for the sub-grid stresses, the sub-grid eddy viscosity ν_t and the sub-grid kinetic energy, k^{sgs} need to be modeled.

A non-equilibrium model[1,4] using a transport equation for the sub-grid kinetic energy, k^{sgs} is used in this study and is given by :

$$\frac{\partial\overline{\rho}k^{sgs}}{\partial t} + \frac{\partial}{\partial x_i}(\overline{\rho}\tilde{u}_i k^{sgs}) = P^{sgs} - \epsilon^{sgs} + \frac{\partial}{\partial x_i}\left(\overline{\rho}\frac{\nu_t}{Pr_t}\frac{\partial k^{sgs}}{\partial x_i}\right) \qquad (8)$$

The terms, P^{sgs} and ϵ^{sgs} in the above equation are respectively, production and dissipation of sub-grid kinetic energy. The sub-grid dissipation, ϵ^{sgs} is obtained by integrating the dissipation spectrum $(D(k) = -2\nu k^2 E(k))$ over the unresolved wavenumbers,[5] to get

$$\epsilon^{sgs} = C_\epsilon(k^{sgs})^{3/2}/\overline{\Delta} \qquad (9)$$

where, $C_\epsilon = 0.916$. The sub-grid production term is modeled as $P^{sgs} = -\tau^{sgs}_{ij}(\partial\widetilde{u}_i/\partial x_j)$. The coefficient Pr_t is the turbulent Prandtl number and is taken to be 0.9. The sub-grid eddy viscosity is modeled as[5]

$$\nu_t = 0.067\sqrt{k^{sgs}}\Delta \tag{10}$$

The coefficients 0.067 (in the expression for ν_t) and 0.916 (in the expression for ϵ^{sgs}) can also be obtained as a part of the solution by using the dynamical procedure, as shown earlier.[6] More information on dynamic modeling can be found elsewhere.[6,7]

2.2 Scalar Transport Closure

In addition to τ_{ij}^{sgs}, several unclosed terms appear in the LES filtered energy and species equations given in Eqn. (4), such as:

$$\begin{array}{lcl} H_i^{sgs} & - & \text{sub-grid enthalpy flux} \\ \sigma_i^{sgs} & - & \text{sub-grid viscous work} \\ Y_{i,k}^{sgs} & - & \text{convective species flux} \\ q_{i,k}^{sgs} & - & \text{sub-grid heat flux} \\ \theta_{i,k}^{sgs} & - & \text{sub-grid species diffusive flux} \end{array} \tag{11}$$

The sub-grid total enthalpy flux H_i^{sgs} is also modeled using the eddy viscosity model as follows:

$$H_i^{sgs} = \frac{-\overline{\rho}\nu_t}{Pr_t}\frac{\partial \tilde{H}_k}{\partial x_i}$$

Note that, since large-scale motion is resolved in LES, the associated counter-gradient processes in the resolved scales are also resolved (even though a gradient closure is employed for H_i^{sgs}). The other unclosed terms like σ_i^{sgs}, $q_{i,k}^{sgs}$ and $\theta_{i,k}^{sgs}$, are often neglected and there exists no model for these terms.[8] These terms are the sub-grid contribution of the molecular diffusive flux and are often neglected assuming that their contributions are small in high Reynolds number flows.[2,3]

The sub-grid convective species flux $Y_{i,k}^{sgs}$, given in equation Eqn. [4] is modeled using the gradient diffusion assumption as follows.

$$Y_{i,k}^{sgs} = \frac{-\overline{\rho}\nu_t}{Sc_t}\frac{\partial \tilde{Y}_k}{\partial x_i}$$

The coefficient Sc_t is the turbulent Schmidt Number, and is taken to be unity. Nevertheless, theory and experiments[9] have shown that this gradient diffusion assumption for species transport can lead to significant errors.

Most of these assumptions for neglecting the sub-grid terms such as $q_{i,k}^{sgs}$ and $\theta_{i,k}^{sgs}$, and the gradient diffusion modeling for $Y_{i,k}^{sgs}$ are often not justifiable. It will be shown that using the LES-LEM approach (to be described in the next section), most of these assumptions can be relaxed and can be elegantly included in the model for sub-grid scalar transport.

2.3 Filtered Reaction Rate Closure

The final term to be modeled in the LES reacting flow equations is the filtered reaction rate term, $\overline{\dot{w}}_k$. The closure for $\overline{\dot{w}}_k$ is complicated due to its highly non-linear nature. Consider a simple global mechanism $F + O \rightarrow P$, for which the production rate of the product can be expressed as

$$\dot{w}_P = AT^b exp(-T_A/T)\rho^2 Y_F Y_O$$

where A, b and T_A are pre-exponential factor, temperature index and the activation energy, respectively. Also, ρ, Y_F, Y_O and Y_P are density, mass fraction of fuel, oxidizer and the products, respectively. Filtering the reaction rate term $\dot{w}_P$ gives rise to higher order correlations of the form, $\overline{\rho Y_F^{"} Y_O^{"}}$, $\overline{\rho Y_F^{"} T^{"}}$, $\overline{\rho T^{"} T^{"}}$, etc., that cannot be ignored in a turbulent reacting flow. Hence, proper treatment of this term is a major research issue in LES of reacting flows. Excellent review on the various modeling approaches used to approximate the $\overline{\dot{w}}_k$ in the context of LES can be found elsewhere.[8] It will be shown that, in the LES-LEM approach (to be described in the next section) the reaction rate term can be computed exactly without any need for a closure.

3 LEM: Sub-grid scalar closure

In Linear Eddy Mixing (LEM) model[10–13] the various physical processes, such as large scale advection, small scale mixing, molecular diffusion and chemical reaction are resolved at their relevant length and time scales.

In LES-LEM the governing filtered conservation equations for mass, momentum and energy are numerically integrated using a time and space accurate numerical scheme on an appropriate three-dimensional grid. It should be noted that the equations for mass, momentum and energy solved on the resolved grid are in the Eulerian form (i.e., Eulerian frame of reference). Attention is drawn to the fact that, at this stage, no conservation equation for species are solved on the resolved LES grid.

The species/scalar field evolution is tracked using a **two-scale** numerical approach. In this technique, turbulent convection of the scalars is split into two parts: **large scale advection** and **turbulent stirring** at the small (sub-grid) scales. Large scale advection is the convection that happens above the unresolved scales. This is modeled by using a Lagrangian scheme which explicitly transports mass across the finite-volume cell surfaces in a manner that is consistent with the mass transport in the Eulerian continuity equation solved on the resolved grid. Small-scale advection is the turbulent stirring by scales smaller than the resolved grid. Note that, turbulent convection at the sub-grid scales only transports fluid mass over sub-grids length scales.

To describe this two-scale numerical method, consider the exact (i.e., unfiltered) evolution equation for a reactive scalar Φ, written in the Eulerian form:

$$\rho\frac{\partial\Phi}{\partial t}+\underbrace{\rho u_i\frac{\partial\Phi}{\partial x_i}}_{\text{C}}+\underbrace{\rho\frac{\partial}{\partial x_i}[-D_\Phi\frac{\partial\Phi}{\partial x_i}]}_{\text{D}}=\underbrace{\dot{w}_\Phi}_{\text{R}} \qquad (12)$$

where term C represents the total (large scale + small scale) convection, term D represents the molecular diffusion and term R represents the chemical reaction source term. Now, split $u_i=(\tilde{u_i}+u_i^{'})$ where, $\tilde{u_i}$ and $u_i^{'}$ are the contribution to the total convection from the resolved (large) and sub-grid (small) scales. By grouping the molecular diffusion and the chemical reaction as small scale processes one can split Eqn. [12] into two equations, one corresponding to the large scale processes and another corresponding to the small-scale processes as follows.

$$\rho\frac{\Phi^*-\Phi}{\Delta t_{LES}}+\underbrace{\rho\tilde{u_i}\frac{\partial\Phi}{\partial x_i}}_{\text{L-C}}=0 \qquad (13)$$

$$\rho\frac{\partial\Phi^*}{\partial t}+\underbrace{\rho u_i^{'}\frac{\partial\Phi^*}{\partial x_i}}_{\text{S-C}}+\rho\frac{\partial}{\partial x_i}[-D_\Phi\frac{\partial\Phi^*}{\partial x_i}]=\dot{w}_{\Phi^*} \qquad (14)$$

where term L-C represents the large scale convection and term S-C represents the small scale convection. Here, Δt_{LES} is the fluid-dynamic/acoustic (LES) time-step and Φ^* is the intermediate solution after the large-scale convection process. The large-scale advection processes (governed by Eqn. [13]) and the small scale advection (in Eqn. [14]) account for the complete evolution of the scalar fields. The small scales range from the grid resolution down to the Kolmogorov (smallest fluid dynamic scale) or Batchelor micro-scale (approximate size of the smallest scalar fluctuation).

In LES-LEM, the small scale processes (sub-grid scale turbulent mixing, molecular diffusion and chemical reaction) are resolved in one-dimension. This idea relies on the following.
(1) small scale turbulence is locally homogeneous and isotropic
(2) Effect of heat-release and the associated thermal expansion on the flow is the same in all direction
(3) the model in its basic form, has been shown[10] to capture the correct physics of scalar mixing at small-scales in homogeneous, isotropic turbulence.

It should be noted that, isotropic behavior required by (1) and (2) are questionable in high Mach number flows, since information does not propagate at equal speeds in all directions. However, for subsonic flows (that are of interest here) it is reasonable.

3.1 Sub-grid LEM simulation

For the purpose of solving Eqn. [14], within each LES cell, a 1-D line segment known as the LEM domain is defined and discretized.

3.1.1 Molecular Diffusion and Chemical Reaction

The 1-D reaction-diffusion equation for the species and the temperature written in non-conservative form are solved numerically on the one-dimensional domain. These equations are given below.

$$\rho\frac{\partial Y_k}{\partial t}+F_{kstir}+\rho\frac{\partial}{\partial s}(-D_k\frac{\partial Y_k}{\partial s})=\dot{\omega}_k W_k \qquad (15)$$

$$\rho c_p\frac{\partial T}{\partial t}+F_{Tstir}-\sum_{k=1}^{N}\rho c_{p,k}D_k(\frac{\partial Y_k}{\partial s})(\frac{\partial T}{\partial s})-\frac{\partial}{\partial s}(\bar{\kappa}\frac{\partial T}{\partial s})=-\sum_{k=1}^{N}h_k\dot{\omega}_k W_k \qquad (16)$$

Here, T, $\bar{p}$ and ρ are the sub-grid temperature, resolved pressure, and the sub-grid mass density, respectively. Y_k, W_k, $c_{p,k}$ and R_u, are the mass fraction, molecular weight, specific heat at constant pressure, and universal gas constant respectively. Density in the sub-grid field is computed using the equation of state for the scalar mixture $\bar{p}=\rho T\sum_{k=1}^{N}Y_kR_u/W_k$ and the caloric relation is given by $h_k=\Delta h^o_{f,k}+\int_{T^o}^{T}c_{p,k}(T')dT'$. Also, $\dot{\omega}_k$, h_k, V_k and $\Delta h^o_{f,k}$ are respectively the mass reaction rate, enthalpy, diffusion velocity and standard heat of formation (at standard temperature, T^o) of the k-th species. $\bar{c}_p$, $\bar{\kappa}$ and D_k are the mixture averaged specific heat at constant pressure and thermal conductivity and mixture averaged diffusivity of the k-th species respectively.

In Eqns. [15] and [16], s denotes the co-ordinate direction on the 1-D domain. The orientation of the 1-D domain is usually aligned in the direction of the maximum scalar gradient.[11] The length of the 1-D domain is taken to be equal to that of the local LES filter width, Δ. Note, that Eqns. [15] and [16] are equivalent to Eqn.[14] written in terms of sub-grid species and temperature field. Turbulent convection at the sub-grid scales of the form $u\partial Y_k/\partial s$ and $u\partial T/\partial s$ are symbolically represented as F_{kstir} and F_{Tstir}, respectively in Eqns. [15] and [16] and these are implemented explicitly, as discussed in the next section.

Assumptions

- Sub-grid pressure (inside the 1-D LEM domain) is assumed to be uniform and same as the resolved grid pressure. In the absence of strong pressure gradient such as those in shocks, and in highly compressible flows, it is reasonable to assume that the pressure in the sub-grid remains constant. However, pressure can vary spatially over the LES (resolved) grid, even though it is assumed to be uniform within the sub-grid.

- The contribution from the sub-grid viscous work is neglected.

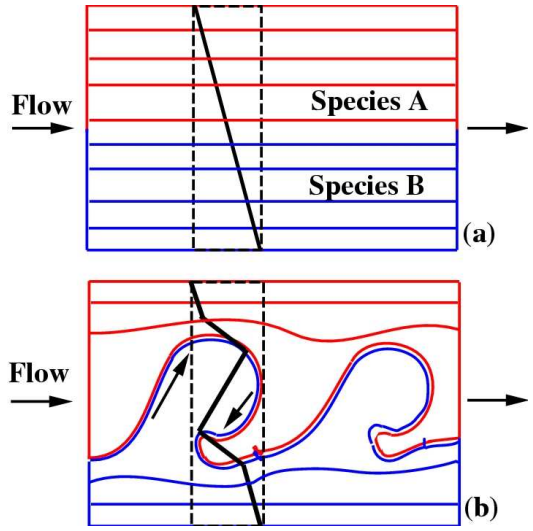

Figure 1 Schematic illustration of the effect of a eddy/vortex roll-up on a two-dimensional scalar field.

- Calorically perfect gas model assumed. But, it is straight-forward to extend LEM for thermally perfect model.
- Radiation effects are neglected in this study. But can be easily included in the model as shown elsewhere.[14]

3.1.2 Sub-grid scale turbulent convection

The effects of the sub-grid velocity field on the sub-grid scalar fields are modeled (numerically) using stochastic re-arrangement events called *triplet maps*.[11] Each triplet map represents the action of an isotropic turbulent eddy on the sub-grid scalar field. The intuitive rationale for adopting the triplet map is illustrated in Fig. 1. Consider a mixing layer configuration shown in Fig. 1(a) with a plane material surface separating species A from species B. The bold straight line running from the top to the bottom shown in the box (dashed line) represents the initial concentration profile (uniform gradient). Horizontal lines (red and blue) represents the concentration isopleths at the initial time. Fig. 1(b) shows the distortion (stretching + compression) of the concentration isopleths due to the action of an eddy or vortex roll-up. The initial linear concentration profile evolves to a form, qualitatively resembling the profile obtained by applying the triplet map to the linear profile. The scalar field produced is continuous and measure preserving (Note: scalar gradient field is not continuous).

Three parameters are needed to implement the turbulent stirring events: eddy size l, the eddy location within the 1D domain and the stirring frequency (mean event rate per unit length of the mapping domain) λ. The eddy size in the range Δ to η (Kolmogorov scale) is determined from an eddy size distribution $f(l)$, obtained using inertial range scaling in three-dimensional turbulence:[11]

$$f(l) = \frac{5}{3}\frac{l^{-8/3}}{(\eta^{-5/3} - \Delta^{-5/3})} \tag{17}$$

Here, η is determined from inertial range scaling law

$$\eta = N_\eta \frac{\Delta}{Re_\Delta^{3/4}} \tag{18}$$

where N_η is an empirical constant and Re_Δ is the sub-grid Reynolds' number based on the sub-grid turbulence intensity, kinematic viscosity and the local LES filter width, Δ. The constant N_η reduces the effective range of scales between Δ and η but does not change the turbulent diffusivity, as described in an earlier study.[15] The event location is randomly chosen from a uniform distribution and the event (mapping) rate (mean frequency per unit length) is[11]

$$\lambda = \frac{54}{5}\frac{\nu Re_\Delta}{C_\lambda \Delta^3}\frac{[(\Delta/\eta)^{5/3} - 1]}{[1 - (\eta/\Delta)^{4/3}]} \tag{19}$$

The time interval between events is then given as

$$\Delta t_{stir} = \frac{1}{\lambda \Delta} \tag{20}$$

where Δ is the length of the 1-D domain, which is also same as the local LES filter width. These mappings are implemented as a Poisson process in time. Note, that λ is not a function of length scale, l (of stirring) which implies that the interval between the stirring events are the same for all the length scales. Strictly speaking this is not true, but the following considerations justify the proposition.
(1) Assumption of the local isotropy in the sub-grid, implies that the range of the stirring length scales are closely spaced in the wave-number space. This implies that their time-scale (or the turn-over time) is nearly same.
(2) The sub-grid Re_Δ and the filter width, Δ are varying spatially over the LES (resolved) grid. This implies that the the range of the stirring length scales and hence, the frequency of the stirring events also vary spatially over the LES (resolved) grid, even though it is same within the sub-grid.

The above formulation has two constants: C_λ and N_η, both of which arise from the use of scaling laws. In the earlier studies,[15,16] these parameters were defined by comparing LEM predictions to experimental data[17] in the flamelet regime. It is argued[18] that the scalar diffusivity due to triplet maps should equal the momentum diffusivity (by triplet maps), since inertial range eddies are responsible for both the processes. Therefore, the same value of the coefficient C_ν used in the expression for eddy viscosity expression (Eqn. [10]), should be used for scalar diffusivity C_λ. This value (0.067) turns out to be close to the

values used in the earlier studies.[15,16] The present study, uses the same constant for all the simulations reported, even though the LDKM approach used here, yields dynamically varying coefficients.

3.1.3 Volumetric Expansion

The final sub-grid process in the LEM, which needs to be described is the volumetric expansion due to heat release. As mentioned earlier, constant pressure is assumed in the sub-grid so that the heat release will cause volume expansion. Since the sub-grid convection terms are modeled explicitly using triplet maps, volumetric expansion must be included explicitly as well. Volumetric gas expansion caused by heat release is modeled by expanding each linear-eddy cell in the sub-grid domain by an amount equal to

$$\Delta V^*_{LEM,i} = \frac{\rho^n_i}{\rho^*_i} \tag{21}$$

where $\Delta V_{LEM,i}$ is the change in volume of LEM cell i. ρ^n_i and ρ^*_i are, respectively, the density of the "$i-th$" cell at the previous and the current time integration levels in the sub-grid simulation (not at the fluid-dynamic time-step, (Δt_{LES}) at LES level). In the previous studies,[18,19] the domain containing the expanded cells is re-gridded so that each cell is returned to its initial volume. In the present study, re-gridding the cells is done after the large-scale advection process, and not at this stage. This is explained in the Section 3.3

3.1.4 Numerical Implementation

An operator splitting method[15,20] is used to integrate the stiff reaction-diffusion equations (Eqns. [15] and [16]). This splitting combines an explicit treatment of the LES resolved mass and momentum equations at the global time step with several explicit fractional steps for diffusion, reaction and turbulent stirring at the sub-grid scales. To solve the Eqns. [15] and [16] numerically, all spatial derivatives are discretized using a second-order accurate central difference schemes and a zero-gradient boundary conditions are imposed for the species and the temperature equations at sub-grid domain boundaries.

LEM-domain (1-D line segment) is initialized in every LES cell with a fixed number of cells. The number of one-dimensional cells is estimated as follows. To represent an eddy using a triplet map, a minimum of 6 points are needed.[21] If the sub-grid Re_Δ is known, then using the expression $\eta = N_\eta \Delta Re_\Delta^{-3/4}$, an estimate of the smallest length scale can be obtained. Then the maximum number of LEM cells needed to completely resolve all the sub-grid scales can be computed using the expression,

$$N_{max} = \min(\frac{\Delta_{ijk}}{\eta_{ijk}}) \tag{22}$$

where Δ_{ijk} and η_{ijk} are the local LES filter width and the Kolmogorov scale at the cell "ijk". The length of the linear eddy domain is set equal to the LES filter width Δ.

3.2 Large-Scale Advection: Splicing

The large-scale advection process governed by Eqn. [13] is implemented in a Lagrangian manner using a technique called **splicing**. It is important to realize that splicing models the large-scale advection process and does not directly solve Eqn. [13] using a finite-difference of finite-volume method. Nevertheless, splicing satisfies the basic condition for the conservation of mass.

After completing the sub-grid LEM simulations in each LES cell, the sub-grid scalar fields are advected by the LES-resolved velocity field, in a Lagrangian sense. This method involves the transfer of LEM cells between the LES control volumes to account for the mass flux across the LES cell faces.

Three quantities are needed for this procedure:

- magnitude or the amount of mass that has to be transported across each of the LES cell faces
- direction of the mass flux (influx or outflux) on each cell face
- ordering/priority of the advection operation for the 3-co-ordinate directions

In a finite-volume scheme, mass flux is known on each of the LES cell faces. In addition, the direction of the velocity field defines the direction of the mass flux on the cell-faces. Hence, the first two of the above mentioned three quantities are taken care of by the resolved grid continuity equation and the momentum equations. The third issue is resolved using the following approach.

In the numerical implementation of the scalar advection, the three dimensional advection operator is approximated by a sequence of three, one-dimensional advection operators. On a general three-dimensional grid the mass transfer from any control volume to any neighboring control volume is also predominantly three-dimensional. As a result, different number of one-dimensional cells are transported in different spatial directions. So the order in which these operators act on the scalar field can have a significant effect on the scalar field evolution. Here, the cells going out in the direction of largest outflux are fluxed out first from the right end of the sub-grid domain. Similarly the largest influx is added first to the left end of one-dimensional domain.

Next step in the large-scale advection process is the identification and actual transport of the linear-eddy cells. This is implemented as follows. Since the mass flux on each of the six control surfaces of a LES cell is known, it can be sorted in an ascending order. Note

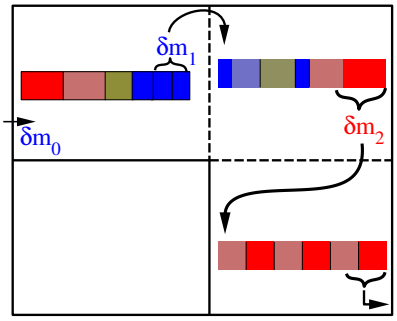

a) Before splicing

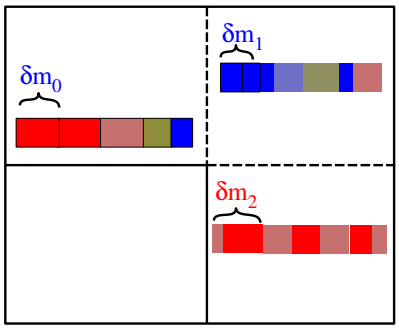

b) After splicing

Figure 2 Schematic diagram illustrating the splicing process.

that, before sorting the following sign-convention is imposed for the face mass-fluxes. Influx is given a positive sign and the outflux is given a negative sign along each co-ordinate directions. Thus, upon sorting, the mass fluxes would be arranged, from the maximum outflux (least negative number) to maximum influx (highest positive number). Now, for each outflux, every LES cell computes the number of one-dimensional cells that contains the mass. Since the density and the volume is known for each one-dimensional cell, the cell mass is computed simply as the product of the cell density times the cell volume. It should be noted that, the amount of mass to be transported across a LES cell surface can be a fraction of the linear eddy cell mass. To transport mass smaller than the cell mass, the following algorithm is used.

- Let the temperature and mass fraction of the linear-eddy cell D be T_D and Y_{k_D}
- Let the density, volume and the mass of the cell D be ρ_D, V_D and Δm_D
- Let the amount of mass to be transported across an LES cell surface be δm
- If $\delta m < \Delta m_D$, then split D into two cells, D_L and D_R such that,
  $\rho_{D_L} = \rho_{D_R} = \rho_D$
  $\Delta m_{D_R} = \delta m$
  $\Delta m_{D_L} = \Delta m_D - \delta m$

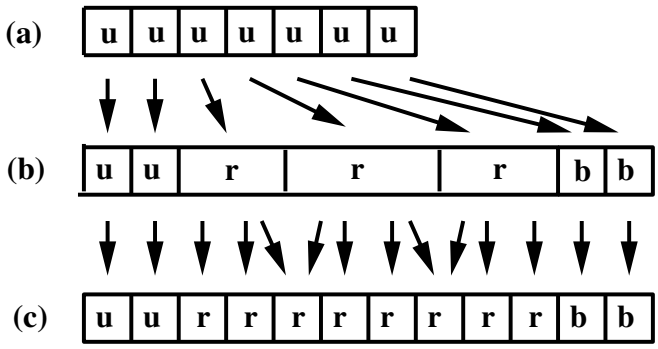

Figure 3 Schematic diagram of the re-gridding procedure used to model volumetric expansion of LEM cells.

$$V_{D_R} = \delta m/\rho_D$$
$$V_{D_L} = V_D - V_{D_R}$$
$$T_{D_L} = T_{D_R} = T_D$$
$$Y_{k_{D_L}} = Y_{k_{D_R}} = Y_{k_D}$$

Figure 2 shows a schematic diagram of the scalar field before and after splicing. Fractional splicing and the non-uniform distribution of the scalar field after splicing is apparent in this schematic diagram.

3.3 Re-gridding the Linear-Eddy domain

Even though splicing conserves mass, it does not conserve the number of linear-eddy cells, due to the convection of fractional cells. So, the number of one-dimensional cells in an LES cell before and after splicing are not the same. Furthermore, volumetric expansion due to heat release and splicing also leads to a non-uniform distribution of the volume of the cells. Since the numerical scheme employed for solving the sub-grid reaction-diffusion equations assumes an uniform grid, it is desirable to re-grid the non-uniform 1-D line segment to an uniform grid. Also, to avoid programming complexities in a parallel environment (e.g. dynamic load balancing), it is desirable to have same number of cells everywhere in the computational domain. So, to equalize the volume of the cells and to retain the same number of cells everywhere in the computational domain, the one-dimensional domain is re-gridded to have cells of equal volume after each splicing. Errors introduced due to the spurious diffusion associated with re-gridding has not been evaluated yet. A schematic diagram of the procedure is shown in Fig. 3. The letters "u", "r" and "b" refers to the unburnt, reacting and completely burnt linear eddy cells, respectively. Figure 3(a) shows the initially uniform linear eddy domain. Chemical reaction and the subsequent thermal expansion causes a non-uniform distribution of the cell volumes, as shown in Fig. 3(b). Re-gridding process, generates a uniform distribution of the volume in the linear eddy cells as shown in Fig. 3(c).

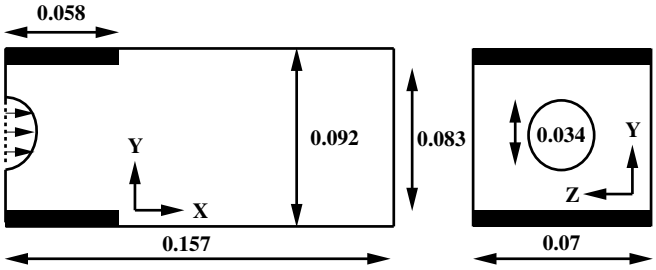

Figure 4 Schematic diagram of the GEAE - LM6000 combustor All dimensions are in meters.

3.4 Large scale and Small scale Coupling

To complete the LES-LEM formulation, the simulated sub-grid field must be coupled to the resolved field variables. The resolved field provides the pressure and the sub-grid kinetic energy to the sub-grid LEM simulation. After the sub-grid simulation, the sub-grid LEM field provides the filtered species, temperature and the specific heats to the resolved field.

Filtered quantities from the sub-grid simulation are computed as follows.

- Let Y_{k_i} be the sub-grid species mass fraction for species 'k' in a cell 'i'
- Let T_i and ρ_i be the sub-grid temperature and density in a cell 'i'
- Sub-grid averaged (filtered)species mass fraction is computed as

$$\widetilde{Y_{k_i}} = \frac{\sum_{i=1}^{N_{LEM}} \rho_i Y_{k_i}}{\sum_{i=1}^{N_{LEM}} \rho_i}$$

- Sub-grid averaged (filtered) temperature is computed as

$$\widetilde{T_i} = \frac{\sum_{i=1}^{N_{LEM}} \rho_i T_i}{\sum_{i=1}^{N_{LEM}} \rho_i}$$

This sub-grid averaged (filtered) temperature is redundant, since the solution of the resolved grid energy equation along with the filtered species (from LEM) gives the actual temperature. The comparison of the two temperatures show that they are in very good agreement with each other. In the present study, the temperature computed from the LES equation is used as the resolved grid temperature. However, the sub-grid temperature field is not altered and it is evolved continuously.

4 Results and Discussion

LM6000 is a rectangular can type combustor with a circular inlet from a premixer/swirler configuration. A schematic diagram of the LM6000 combustor is shown in Fig. 4 At the inlet a highly swirling jet (Swirl number [1]of 0.56) is injected at high pressure (6 atm.) and

[1]Swirl number is defined as the ratio of axial flux of angular momentum to that of axial flux of the axial momentum itself

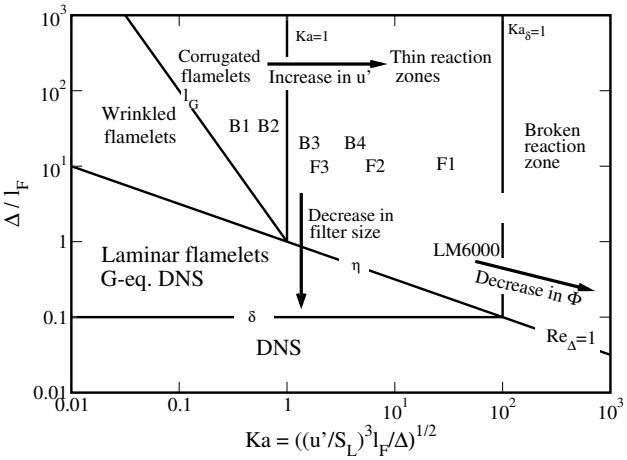

Figure 5 Regime diagram for the LES of turbulent premixed combustion.

with a pre-heated temperature of 644 K. The dark region at the top and bottom part of the combustor shown in Fig. 4 are the blowing sections. These sections are provided to cool the optical window used for measurements. In the present study, similar to the previous studies[6, 22] hot products were injected through the blowing sections.

The conditions specified at the inlet are the axial, radial and tangential velocities and the turbulent kinetic energy. The inlet velocity profile determines the Swirl number which in turn determines the key flow-field characteristics such as the formation of the *Vortex Break-down* phenomenon, location of the frontal stagnation point, the extent of the reverse mass flow and the strength of the external recirculation zone. These features in turn determine the flame location and the heat release. Thus, the accurate specification of the inlet conditions is a key-requirement for the correct prediction of the flow-fields. In the present study, the mean velocity profiles provided by the GEAE company are used at the inlet and are same as the profiles used in the earlier studies.[6, 22]

The only information provided about the inflow turbulence is the intensity of the incoming turbulence, and it is set equal to 7% in the present study. The Reynolds number based on the inlet diameter is 320,000.

Recently, a new regime diagram for premixed combustion was proposed,[23] which distinguishes the effects of turbulence/chemistry interaction and the numerical treatment of LES. The consequences of changing the LES filter width and its effect on the physical mode of combustion (corrugated flamelet, thin-reaction zones broken reaction zone etc,.) are clearly shown in the diagram. Figure 5 shows the new regime diagram along with the locations of the various flames investigated in the past.[15, 24]

Based on the flow conditions, the present flame (indicated as LM6000) is identified to be within the thin-

reaction zones regime, as shown in Fig 5.

No-slip, adiabatic wall boundary conditions are used for the combustor's walls. Characteristic boundary conditions were used for the subsonic inflow and outflow.[25] A structured rectangular computational grid that uses 151 × 118 × 92 points is employed in the present study. The present finite-volume solver uses an embedded boundary method for handling the circular inflow in a Cartesian rectangular grid.[26] The embedded boundary method is based on setting the values of the state vector at particular locations (in the finite volume cells) inside the solid body in such a way that the wall boundary conditions are satisfied. This method offers several advantages. The main one is its ability to manage complex geometries. In the case of a gas turbine combustor, since the geometry is circular in nature, a traditional approach will require a cylindrical grid, which will yield acceptably accurate results except for the centerline region where the gradients will tend to infinity as the radius tends to zero. An alternate method, the unstructured grid approach, will be able to handle the centerline problem, but will have overwhelming computational requirements, both in terms of CPU time, and of memory. The present method avoids this cost.

Another advantage of the method is the fact that it allows the numerical scheme to employ a Cartesian grid irrespective of the complexity of the geometry involved. This allows for orthogonal cells, which diminishes the numerical error and improves the stability of the numerical solution. In addition, the aspect ratio of the cells is much easier to control. More details about the embedded grid approach can be found elsewhere.[26]

Three simulations are performed to compare and contrast the features of the LES-LEM simulations. The first simulation employs the dynamic-LES with a G - equation flamelet approach. This has been studied earlier,[22] and hence for the sake of brevity, details are not given here. The second simulation employs the LES-LEM approach described in the previous section using a single-step, 5-species finite-rate mechanism.

The presence of high shear and turbulent strain rates near the shear layer of the combustor inlet, suppresses the reaction rates greatly in these regions. In such a situation the flame lifts off from the inlet. However, high swirling flow creates the Vortex Break-down (VB) bubble along the axial direction, and therefore, the lifted flame is not blown off but is stabilized upstream of the recirculation region.

To model this lift-off effect, a third simulation using LES-LEM was carried out. Since, the single-step global chemistry employed in the present study cannot predict flame liftoff, an extinction criteria based on the strain-rate is used to modify the reaction rates. It has been reported[27] that the critical value of strain-rate at flame extinction for a 4-step methane-air mechanism is 547 sec^{-1}. To account for the presence of the swirl, an extinction strain-rate of 400 sec^{-1} is used and in regions where the strain rate exceeds this value, the local reaction rate is forced to zero. It should be noted that, this study is only qualitative and is used to show that lift-off can be modeled using LES-LEM and cannot be done easily using the G - equation approach. These three simulations are identified as G-EQN, LES-LEM and LES-LEM-EXT, respectively.

Before sampling the data for statistics, the flow was evolved for approximately 2 flow through times. All the results presented in this section are ensemble averaged over 5 flow through times based on the mean center-line axial velocity at the inlet. All the velocity profiles shown are non-dimensionalized by the center-line velocity at the inlet U_O and the distance are non-dimensionalized by the inlet diameter D.

The current simulations were carried out on a distributed memory parallel processing computers (Cray-T3E, 1200 MHz) using the Message Passing Interface (MPI). Typically 160 processors were employed for present simulations. For the present simulation using $\approx$ 1.6 million LES grid points and 12 LEM cells per LES cell, it required 3840 single processor hours on the Cray T3E per flow through time. The LEM resolution ($\Delta_{LEM} = \Delta_{LES}/12$) used here resolves the flame thickness, δ_F with 23 ($= \delta_F/\Delta_{LEM}$) points, adequate enough to resolve the flame-turbulence interaction. It should also be noted that the LES-LEM without chemistry (scalar mixing alone) is very efficient and it is only 10 % of the total cost. It is the stiff chemistry integration that makes the simulation expensive. The memory requirements is 2.4 Gigabytes.

4.1 Mean Velocity Profiles

Figure 6 shows the variation of the axial mean velocity along the center-line of the combustor. The flow evolution is very similar to that of a swirling decaying jet. The swirl imparted to the flow at the inlet causes the familiar *Vortex Break-down* phenomenon when the ratio of the azimuthal to axial velocity exceeds certain level (of order unity). A predominant feature of the VB is the abrupt deceleration of the flow near the axis leading to the formation of a stagnation point and a recirculation bubble that stabilizes the flame.

Comparison of the center-line axial velocity variation shows that both the combustion models (LES-LEM and G-LES) show reasonable agreement with the experimental data. Considering the fact that these simulations were done without any need for ad-hoc adjustments, this level of agreement is considered reasonable.

Figures 7(a),(b) and (c) shows the contours of the axial velocity in the LM6000 combustor predicted using G-EQN, LES-LEM with and without the strain-induced extinction. The location of the VB is marked by the dark-blue contours around the center-line. The

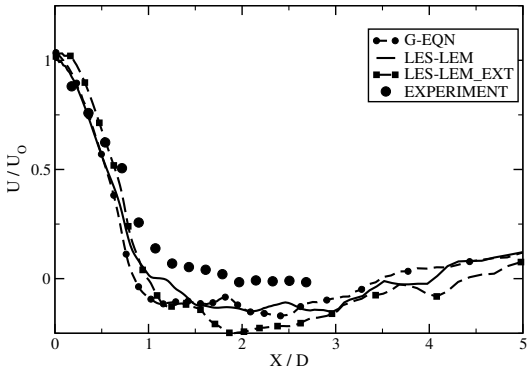

Figure 6 Center-line variation of mean axial velocity

presence of the lifted flame (LES-LEM-EXT) causes strong flame-flow interactions as can be observed from Fig. 7(c). Even though the forward stagnation point of the V-B ($X/D \approx 1$) predicted by LES-LEM and LES-LEM-EXT are the same, the flow reversal occurs faster in LES-LEM-EXT, and hence a stronger flow reversal occurs in the presence of the lifted flame. It can also be observed the region of break-down is asymmetric and extends far downstream. The extent of VB predicted in experiment was $\approx$ 1 diameter. The axial extent of the VB predicted by LES-LEM is 2.2 diameters, whereas the G-LES predicts it to be 2.7 diameters. The reason for the over-prediction of the extent of the V-B zone may be attributed to the incorrect inlet radial velocity profiles or to the error in the LDV measurements in the recirculating flows. Even though the same profiles are used in the present study, it is not necessary that the boundary conditions (inlet velocity profiles) that give a certain solution in RANS should provide a similar solution in LES. RANS solutions are inherently dissipative and its prediction are not reliable in the presence of swirl and stream-line curvature. Hence, the inlet radial profiles used in RANS,[28] that gave good agreement with the experiments need not be the correct inlet velocity profile that was observed in the experiments.

Figure 8 shows the radial profiles of axial velocity at $X/D = 0.18$ predicted using G-LES, LES-LEM and LES-LEM-EXT. It can be observed that the LES-LEM with extinction predicts a better shear layer spread compared to the G-LES. The lifted flame causes a stronger axial flow deceleration, as explained earlier, which widens the shear layer.

Figures 9(a) and (b) show respectively, the mean radial velocity profiles at $X/D = 0.18$ and 0.72. The over-all agreement of both models are good.

Figures 10(a) and (b) show respectively, the radial profiles of the non-dimensionalized mean tangential velocity. Both G-LES and LES-LEM predict peaks at r/D $\approx \pm$ 0.38 similar to those in the experiments. Earlier study[22] using the G-Equation also showed similar peaks and it was attributed to the in-adequate resolution of the inlet velocity profile measurements by GEAE. The overall prediction of the mean velocity fields, (U,V, and W components) by LES-LEM is in good agreement with the LDV measurements and the G-LES approach.

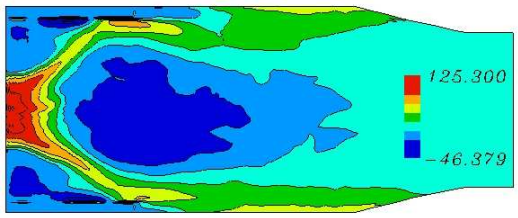

a) G-EQN

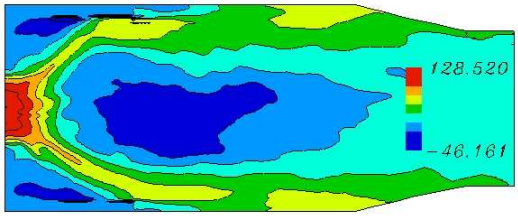

b) LES-LEM

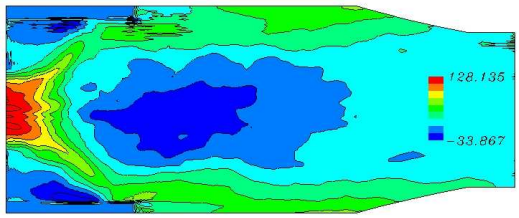

c) LES-LEM with Extinction

Figure 7 Mean axial velocity contours.

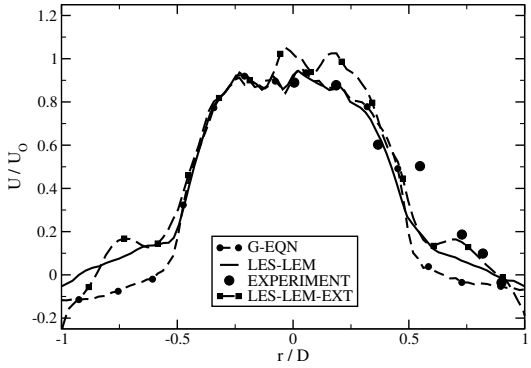

Figure 8 Radial variation of mean axial velocity profiles.

4.2 RMS Velocity Profiles

Figure 11(a) shows the RMS profiles of the axial velocity, u' along the center-line of the combustor. Even though both G-LES and LES-LEM under predicts the peak turbulence, LES-LEM shows a closer agreement

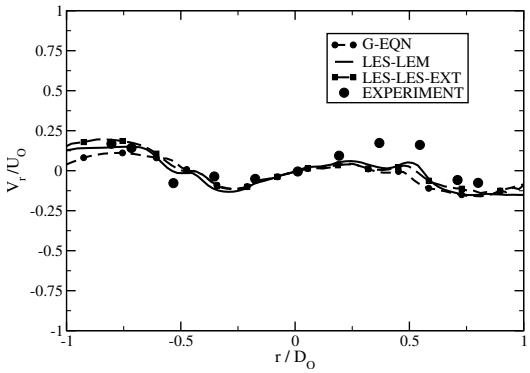

a) X/D = 0.18

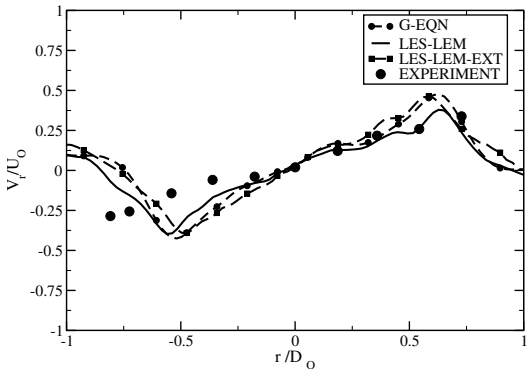

b) X/D = 0.72

Figure 9 Radial variation of mean radial velocity profiles.

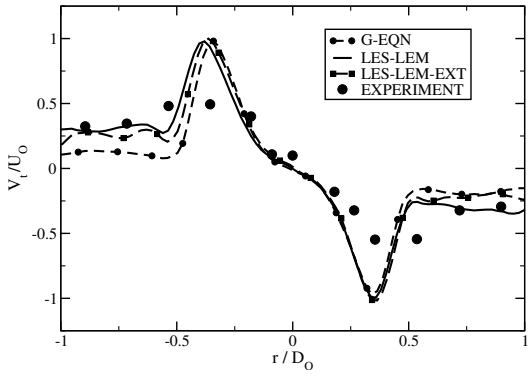

a) X/D = 0.18

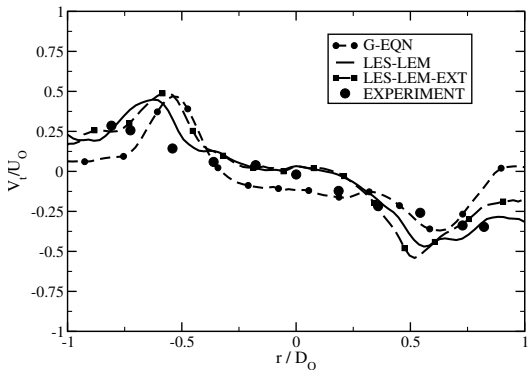

b) X/D = 0.72

Figure 10 Radial variation of mean tangential velocity profiles.

than the G-LES and LES-LEM-EXT. Moreover, LES-LEM (without the extinction) predicts the rise in u' at $X/D \approx 1$, as seen in the experiments. This corresponds to the location at which the flame crosses the center-line of the combustor. Flow acceleration through the flame enhances the turbulence and hence increases the RMS of the axial velocity fluctuations. In case of LES-LEM-EXT, the strong deceleration of the mean axial flow in front of the lifted flame diverts the flow around the flame towards the shear layer and reduces the turbulence intensity near the center line. However as noted earlier the extinction approach used in LES-LEM-EXT is a qualitative model and cannot be used to make any quantitative predictions.

Figure 11(b) shows the RMS profiles of the axial velocity, u' at a radial location ($r/D = 0.81$) near the shear layer. Again the magnitude and the trend of LES-LEM prediction is in very good agreement with the experiments. G-LES and LES-LEM-EXT over-predicts the magnitude of the turbulence intensity along the shear layer. In the case of LES-LEM-EXT, the asymmetric nature of the lifted flame creates a stronger turbulence levels near the shear layer.

Figures 12(a) and 13(a) show respectively, the instantaneous and mean iso-surface of temperature, obtained using G-LES and LES-LEM approach. Magnitude of the iso-surface shown corresponds to $T = 1800$ K. Intense wrinkling of the flame surface due to turbulent eddies can be observed. The formation of rib-like structure at the base of the flame (Fig. 12(b) and 13(b)) clearly shows the effect of swirl on the flame structure. Swirl imparted to the flame, creates a wide, but short flame that spans approximately 1/3-rd of the length of the combustor. LES-LEM seems to predict a more compact flame compared to G-LES in both the mean and the instantaneous snap-shots. Figure 12(c) and 13(c) shows the temperature contours at the mid-plane in the spanwise direction.

Figures 14(a) and (b) show respectively, the perspective and side view obtained using the LES-LEM-EXT (lifted flame) simulation. The flame is seen to stabilize at the forward tip of the V-B encompassing the recirculation zone. The flame base stabilizes at positions where the instantaneous strain rates are low. Figures 15(a), (b) and (c) show respectively the instantaneous temperature contours obtained from G-EQN, LES-LEM and LES-LEM-EXT at a spanwise (midway) location. The lifted flame being stabilized at the central recirculation zone is apparent in this figure. This shows that the simple model using the extinction strain rate criteria in LES-LEM captures some of the the physics of the lifted flame.

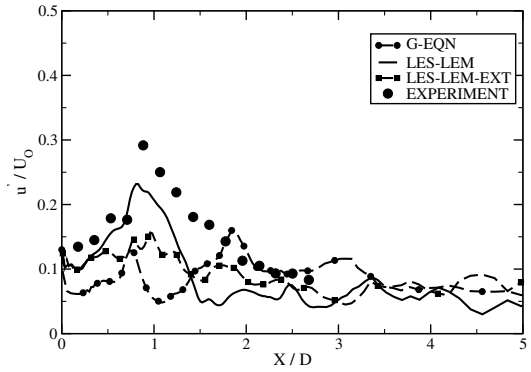

a) r/D = 0.0

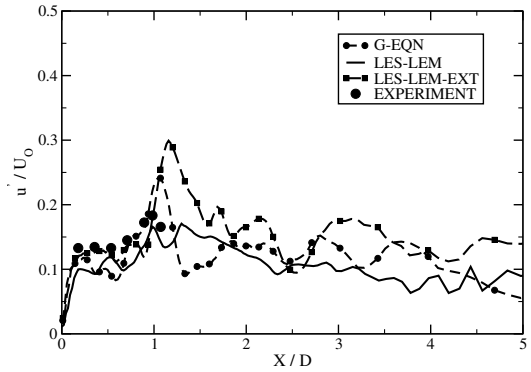

b) r/D = 0.81

Figure 11 Axial variation of RMS axial velocity profiles.

5 Conclusions

A sub-grid turbulent combustion model, LES-LEM is used to predict reactive flow-field in a realistic combustor. The results obtained from the LES-LEM approach is compared with LDV measurements and another combustion model, G-LES approach which has been validated in the past.[22] LES-LEM performs reasonably well in predicting the complex high Re, swirling, compressible, reactive flow-field encountered in this combustor. GEAE's operational hardware (LM6000 DLE combustor). A simple model based on extinction strain-rate used in LES-LEM is shown to capture qualitatively the flame lift-off even with a single-step chemistry. The approach presented here is more robust and physically intuitive, and can capture the flame turbulence interactions at all scales without any need for ad-hoc adjustments that depend on the regime of the combustion.

Acknowledgments

This work was supported in part by the Army Research Office (ARO). Computational time was provided by DOD High Performance Computing Centers at NAVO (MS), and ERDC (MS) under a ARO HPC Grand Challenge Projects.

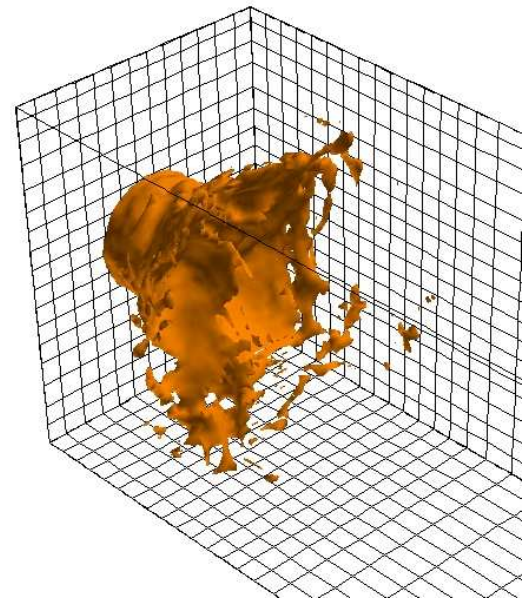

a) Instantaneous G-LES

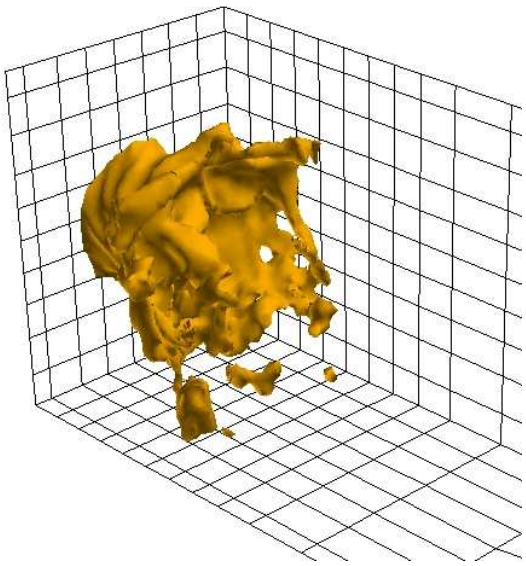

b) Instantaneous LES-LEM

Figure 12 Instantaneous flame structure.

References

[1] Schumann, U., "Subgrid Scale Model for Finite Difference Simulations of turbulent Flows in Plane Channels and Annuli," *Journal of Computational Physics*, Vol. 18, 1975, pp. 376–404.

[2] Fureby, C., *On Modelling of Unsteady Combustion utilizing Continuum Mechanical mixture Theories and Large Eddy Simulations*, Ph.D. thesis, Lund Institute of Technology, Sweden, 1995.

[3] Veynante, D. and Poinsot, T., "Reynolds Averaged and Large Eddy Simulation Modelling for Turbulent Combustion," *New Tools in Turbulence*

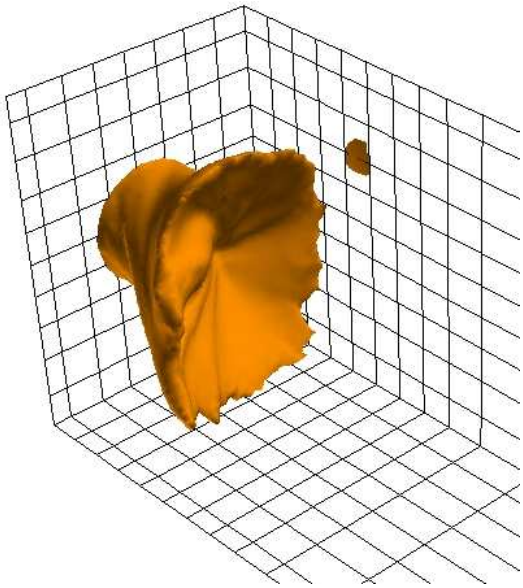

a) Mean G-LES

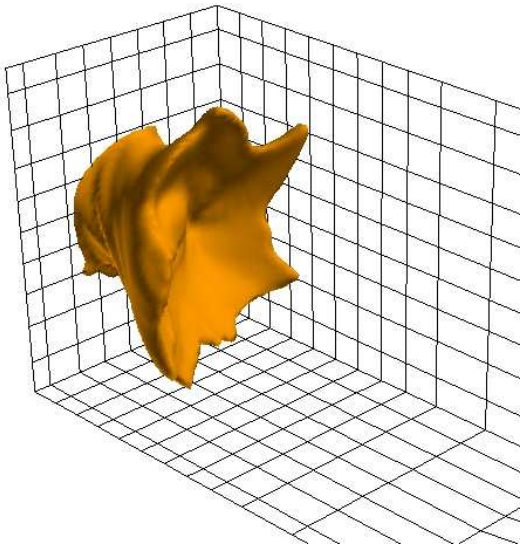

b) Mean LES-LEM

Figure 13 Instantaneous flame structure

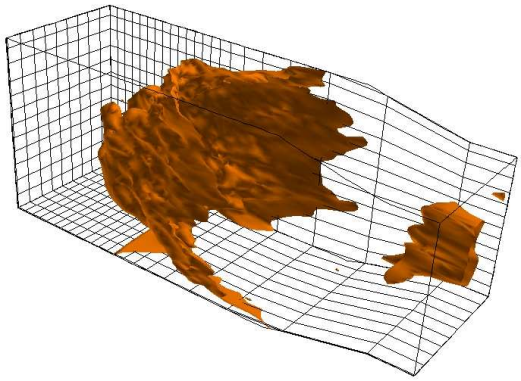

a) Perspective View

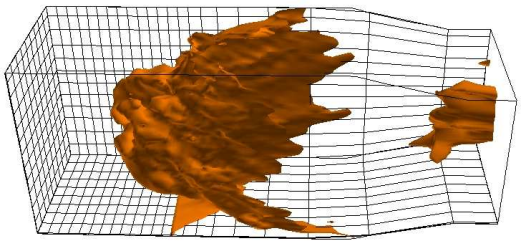

b) Side View

Figure 14 Mean flame structure using LES-LEM-EXT

ModeLling, edited by O. Metais and J. Ferziger, Springer-Les Editions De Physique, 1996.

[4] Menon, S., Yeung, P.-K., and Kim, W.-W., "Effect of Subgrid Models on the Computed Interscale Energy Transfer in Isotropic Turbulence," *Computers and Fluids*, Vol. 25, No. 2, 1996, pp. 165–180.

[5] Chakravarthy, V. and Menon, S., "Large-Eddy Simulations of Turbulent Premixed Flames in the Flamelet Regime," *Combustion Science and Technology*, Vol. 162, 2001, pp. 175–222.

[6] Kim, W.-W., Menon, S., and Mongia, H. C., "Large Eddy Simulations of a Gas Turbine Combustor Flow," *Combustion Science and Technology*, Vol. 143, 1999, pp. 25–62.

[7] Kim, W.-W. and Menon, S., "A New Incompressible Solver for Large-Eddy Simulations," *International Journal of Numerical Fluid Mechanics*, Vol. 31, 1999, pp. 983–1017.

[8] Poinsot, T. and Veynante, D., *Theoretical and Numerical Combustion*, Edwards, Inc., 2001.

[9] Dimotakis, P. E., "Turbulent Free shear layer Mixing," *AIAA-89-0262*, 1989.

[10] Kerstein, A. R., "Linear-Eddy Model of Turbulent Scalar Transport and Mixing," *Combustion Science and Technology*, Vol. 60, 1988, pp. 391–421.

[11] Kerstein, A. R., "Linear-Eddy Model of Turbulent Transport II," *Combustion and Flame*, Vol. 75, 1989, pp. 397–413.

[12] Kerstein, A. R., "Linear-Eddy Modeling of Turbulent Transport. Part 6. Microstructure of Diffusive Scalar Mixing Fields," *Journal of Fluid Mechanics*, Vol. 231, 1991, pp. 361–394.

[13] Kerstein, A. R., "Linear-Eddy Modeling of Turbulent Transport. Part V: Geometry of Scalar Interfaces," *Physics of Fluids A*, Vol. 3, No. 5, 1991, pp. 1110–1114.

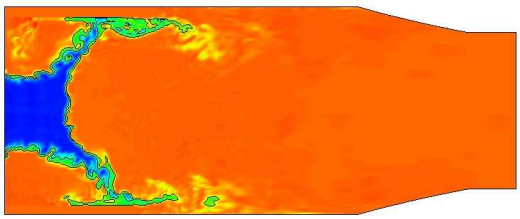

a) G-EQN

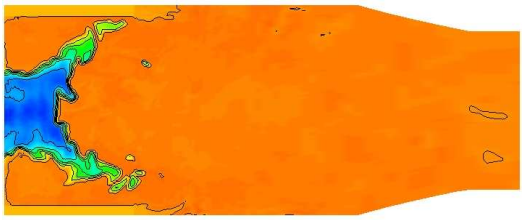

b) LES-LEM

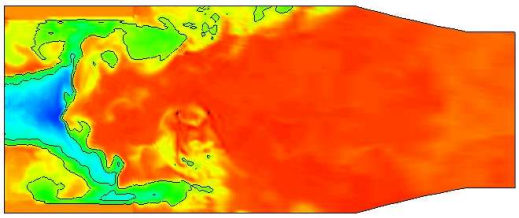

c) LES-LEM-EXT

Figure 15 Instantaneous temperature contours

[14] Zimberg, M. H., Frankel, S. H., Gore, J. P., and Sivathanu, Y. R., "A Study of Coupled Turbulent Mixing, Soot Chemistry and Radiation Effects Using the Linear Eddy Model," *Combustion and Flame*, Vol. 113, 1998, pp. 454–469.

[15] Smith, T. and Menon, S., "One-Dimensional Simulations of Freely Propagating Turbulent Premixed Flames," *Combustion Science and Technology*, Vol. 128, 1996, pp. 99–130.

[16] Smith, T. M. and Menon, S., "Model Simulations of Freely Propagating Turbulent Premixed Flames," *Proceedings of the Combustion Institute*, Vol. 26, 1996, pp. 299–306.

[17] Abdel-Gayed, R. G., Al-Khishali, K. J., and Bradley, D., "Turbulent Burning Velocities and Flame Straining in Explosions," *Proceedings of the Royal Society London A*, Vol. 39, 1984, pp. 393–414.

[18] Chakravarthy, V., *Stochastic Subgrid Modeling of Turbulent Premixed Flames*, Ph.D. thesis, Georgia Institute of Technology, Atlanta, GA, March 2000.

[19] Smith, T., *Unsteady Simulations of Turbulent Premixed reacting flows*, Ph.D. thesis, Georgia Institute of Technology, Atlanta, GA, March 1998.

[20] Calhoon, W. H., Menon, S., and Goldin, G., "Comparison of Reduced and Full Chemical Mechanisms for Nonpremixed Turbulent H2-Air Jet Flames," *Combustion Science and Technology*, Vol. 104, 1995, pp. 115–141.

[21] Menon, S. and Calhoon, W., "Subgrid Mixing and Molecular Transport Modeling for Large-Eddy Simulations of Turbulent Reacting Flows," *Proceedings of the Combustion Institute*, Vol. 26, 1996, pp. 59–66.

[22] Kim, W.-W. and Menon, S., "Numerical Modeling of Turbulent Premixed Flames in the Thin-Reaction-Zones Regime," *Combustion Science and Technology*, Vol. 160, 2000, pp. 119–150.

[23] Pitsch, H. and Duchamp De Lageneste, L., "Large-Eddy SImulation of Premixed Turbulent Combustion using a Level-Set Approach," *Proceedings of the Combustion Institute*, Vol. 29, 2002, pp. 2001–2008.

[24] Chen, Y. C., Peters, N., Schneemann, G. A., Wruck, N., Renz, U., and Mansour, M. S., "The Detailed Structure of Highly Stretched Turbulent Premixed Methane-Air Flames," *Combustion and Flame*, Vol. 107, 1996, pp. 223–244.

[25] Poinsot, T. and Lele, S., "Boundary Conditions for Direct Simulations of Compressible Viscous Flow," *Journal of Computational Physics*, Vol. 101, 1992, pp. 104–129.

[26] Peskin, C. S., "The Immersed Boundary Method," *Acta Numerica*, Vol. 11, 2002, pp. 479–517.

[27] Chelliah, H. K., Seshadri, K., and Law, C. K., "Reduced Kinetic Mechanisms for Applications in Combustion Systems," *Lecture Notes in Physics*, edited by N. Peters and B. Rogg, Springer-Verlag, 1992, pp. 224–240.

[28] Hura, H. S., Joshi, N. D., Mongia, H. C., and Tonouchi, J., "Dry Low Emission Premixer CCD Modelling and Validation," *ASME-98-GT-444*, 1998.